JOURNAL OF MATERIALS SCIENCE 31 (1996) 4055–4065

Elevated temperature deformation behaviour of multi-phase Ni–20 at % Al–30 at % Fe and its constituent phases

S. GUHA*, I. BAKER
Thayer School of Engineering, Dartmouth College, Hanover, NH 03755, USA
P. R. MUNROE
School of Materials Science and Engineering, University of New South Wales, Kensington, New South Wales 2052, Australia

The mechanical behaviour of the multi-phase ($\beta' + \gamma/\gamma'$) alloy Ni–20 at % Al–30 at % Fe and alloys similar to its constituent β' and γ/γ' phases, Ni–30 at % Al–20 at % Fe and Ni–12 at % Al–40 at % Fe, respectively, were investigated. When tested in tension at 300 K, the alloys exhibited $\approx$ 20%, 2% and 28% elongation, respectively. At elevated test temperatures (700, 900 and 1100 K), the multi-phase alloy exhibited increased ductility, reaching an elongation in excess of 70% at 1100 K without necking or fracture. Similarly, the β' alloy demonstrated increased ductility with increasing test temperatures. In contrast, the γ/γ' alloy showed greatly reduced ductility with increasing temperature and was quite brittle both at 900 and 1100 K. Thus, whilst at room temperature the γ/γ' phase improved the ductility of the $\beta' + \gamma/\gamma'$ aggregate, at elevated temperatures the β' phase alleviated the brittleness of the γ/γ' phase, thereby preventing any embrittlement of the multi-phase alloy over the temperature range 300–1100 K. Also, whilst the β' phase improved the room-temperature strength of the multi-phase alloy, at elevated temperatures where the β' phase is known to be weak, the γ/γ' phase improved the strength of the multi-phase alloy up to 900 K, beyond which the strength deteriorated due to disordering and lack of anomalous strengthening in the γ/γ' component.

1. Introduction

Binary, off-stoichiometric compositions of NiAl exhibit brittle behaviour at room temperature, which is in contrast to $\sim$ 2% tensile elongation observed for the stoichiometric compound [1–4]. One demonstrated approach to improve the ambient ductility of NiAl is to alloy it with iron; the β' (ordered bcc B2-structured) (Ni, Fe)(Fe, Al) compound Ni–30Al–20Fe (compositions in atomic per cent) can exhibit up to 6% tensile elongation along with a high yield strength of 800 MPa [5, 6]. An alternative approach is to add a more ductile phase; the multi-phase intermetallic Ni–20Al–30Fe with a second phase, i.e. γ/γ' $(Ni, Fe)_3(Al, Fe)$ added to the β'(Ni, Fe)(Fe, Al) phase resulted in $\sim$ 20% room-temperature elongation [7, 8]. The room-temperature structure–property relationships in the multi-phase compound Ni–20Al–30Fe have been explained in terms of those of its constituent phases, based on results of mechanical testing, examination of deformed microstructures [8], and *in situ* TEM straining experiments [9]. In order to understand fully the structure–property relationships for the multi-phase ($\beta' + \gamma/\gamma'$) alloy, Ni–20Al–30Fe, its elevated temperature (i.e. 700, 900 and 1100 K) mechanical behaviour was studied and related to that of alloys of compositions similar to its constituent β' and γ/γ' phases, Ni–30Al–20Fe and Ni–12Al–40Fe, respectively. The microstructures of the three alloys at each test temperature have been described elsewhere [10]. This paper compares the mechanical behaviour of the three alloys over the temperature range 300–1100 K and relates the multi-phase alloy behaviour to those of its constituent phases.

2. Experimental procedure

The multi-phase, β' and γ/γ' alloys investigated here were processed through a casting plus double-extrusion route; the processing details have been published elsewhere [8]. The high-temperature strengths of the alloys were characterized by both Vickers hot hardness measurements and tensile testing. For hot hardness measurements, cylinders 3 mm in diameter and of 3 mm length, were indented with a sapphire indentor using a 500 g load with a dwell time of 10 s, over a range of temperatures from 300 to $\approx$ 1200 K. An

* *Present address*: MER Corp., 7960 S. Kolb Rd., Tucson, AZ 85706, USA.

0022–2461

average of seven indentations were made at each temperature. The specimen temperature was monitored by a thermocouple attached to the specimen surface. A helium atmosphere was used inside the test chamber for temperatures up to $\approx$ 1000 K; tests at higher temperatures were carried out in vacuum. Tensile tests of Ni–20Al–30Fe, Ni–30Al–20Fe and Ni–12Al–40Fe were carried out in air at 700, 900 and 1100 K (with the exception of the β′ phase which was tested only at 900 and 1100 K) at initial strain rates of $\approx 1 \times 10^{-4}\,s^{-1}$ (crosshead speed of 0.025 mm min^{-1}). Tensile specimen preparation has been described elsewhere [5, 7]. Thermal gradients across the specimens were minimized to $\pm$ 2 K by positioning three thermocouples at the shoulders and the middle of the specimen and adjusting the power input to the three zones of the furnace. Following testing, the furnace clamshells were removed and specimens cooled rapidly in a stream of forced air to prevent any static recrystallization of the microstructures. The fracture surfaces and polished longitudinal sections from tensile specimens were examined using both optical microscopy and scanning electron microscopy (SEM), and deformation structures were examined using transmission electron microscopy (TEM). Specimen preparation techniques for both optical microscopy and TEM have been described elsewhere [10].

3. Results

3.1. Hot hardness tests

The room-temperature microstructure of the double-extruded multi-phase alloy used in these experiments consisted of a $\sim$ 20 μm pro-eutectic β′ constituent within a fine scale (0.5 μm lamellae width) β′γ/γ′ eutectic [8]. Despite its fine scale, the microstructure of the multi-phase alloy was found to be resistant to coarsening up to 1273 K for an annealing time of 195 min [10], which is longer than the duration of a typical tensile test or hot hardness test.

The hot-hardness measurements of the multi-phase alloy, Ni–20Al–30Fe, and β′ alloy, Ni–30Al–20Fe, (see Fig. 1) indicate a behaviour similar to that commonly noted for NiAl [11, 12], and for B2 alloys in general [13], where a significant loss of strength with increasing temperatures occurs beyond either a plateau region or slow decrease in strength in the temperature range $\approx$ 300–673 K (i.e. $T < 0.4\ T_m$. The transition temperature, T_t, beyond which the strength decreases sharply, scales with the solidus temperature, suggesting that diffusion-assisted mechanisms are responsible for such a decrease in strength. Thus, β′ Ni–30Al–20Fe, which has a lower solidus temperature than stoichiometric NiAl (1670 K [7] versus 1991 K [14]), exhibits a lower T_t ($\approx$ 750 K) than stoichiometric NiAl ($\approx$ 900 K) [12]. The γ/γ′ alloy, Ni–12Al–40Fe (Fig. 1), while exhibiting a lower hardness that the β′ phase at lower temperatures (< 673 K), retained its strength up to 973 K, beyond which a sharp decrease in strength was observed, presumably due to coarsening of the γ′ precipitates which was observed microstructurally (see [10]) and eventually disordering/dissolution of γ′ into γ. It should be noted that, although a positive temperature dependence of strength is usually observed for γ′-based alloys, no such anomalous strengthening was observed for this particular γ/γ′ alloy. The rate of loss of strength at temperatures greater than 673 K was lower for the multi-phase alloy than for the single-phase β′ alloy, presumably due to contributions from the high-temperature strength of the γ/γ′ phase.

3.2. Elevated temperature tensile tests

The stress–strain graphs of the elevated temperature tensile tests are shown in Figs 2–4 and the results are summarized in both Table I and Fig. 5.

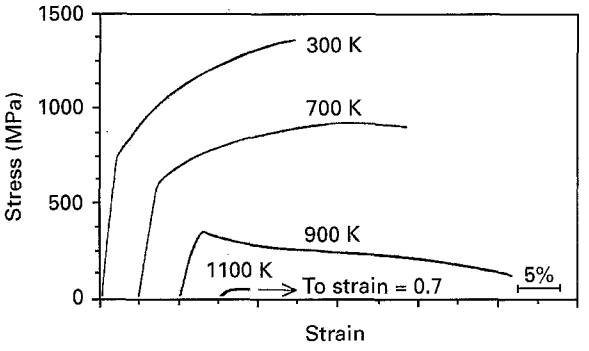

Figure 2 Stress–strain curves of multi-phase (β′ + γ/γ′) alloy, Ni–20Al–30Fe tested at 300 K [1], 700, 900 and 1100 K.

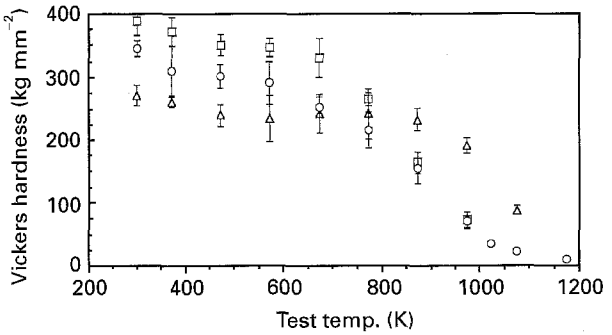

Figure 1 Hot hardness measurements of (○) multi-phase alloy Ni–20Al–30Fe, (□) β′ alloy Ni–30Al–20Fe and (△) the γ/γ′ alloy Ni–12Al–40Fe. Error bars indicate 95% confidence interval.

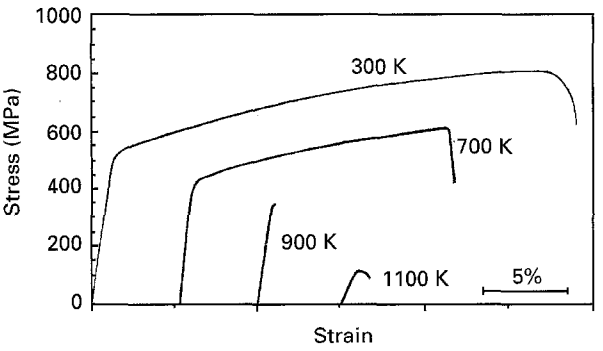

Figure 3 Stress–strain curves of γ/γ′ alloy Ni–12Al–40Fe tested at 300 K [1], 700, 900 and 1100 K.

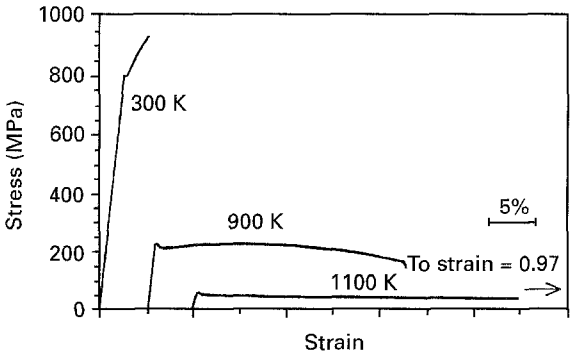

Figure 4 Stress–strain curves of β′ alloy Ni–30Al–20Fe tested at 300 K (after [1]), 900 and 1100 K.

TABLE I Summary of elevated temperature behaviour

Test temperature (K)	Yield stress (MPa)	Fracture stress (MPa)	Plastic strain %
Ni–20Al–30Fe (β′ + γ/γ′)			
300 [1]	760	1350	20
700	610	930	34
900	310	345	41
1100	50	–	> 70[a]
Ni–12Al–40Fe (γ/γ′)			
300 [1]	507	812	28
700	417	617	15
900	–	345	0
1100	119	100	1
Ni–30Al–20Fe (β′)			
300 [1]	800	930	2
900	199	124	27
1100	53	–	97

[a] Test stopped after 70% elongation.

Fig. 2 shows the stress–strain curves of the multi-phase alloy for different test temperatures (the data for 300 K [8] are also included for comparison). At room temperature, the alloy exhibited a yield strength, σ_y, of 760 MPa and plastic strain to fracture, ε_f, of $\approx 20\%$. At 700 K, the yield strength decreased to 610 MPa and ε_f increased to $\approx 41\%$; no work-hardening was observed at this temperature. At 300 K failure preceded necking, whilst at 700 and 900 K slight necking was observed before final failure. Finally, at 1100 K where the microstructure is known to be β′ + γ only [10], no work-hardening was observed after yielding at ≈ 50 MPa, and an elongation of 70% without any necking was observed before the test was stopped. The large elongation without any necking is indicative of the occurrence of either dynamic recovery or dynamic recrystallization. A second sample was strained in vacuum at 1100 K where an ε_f of almost 100% was observed.

Fig. 3 shows the stress–strain curves for the γ/γ′ alloy, Ni–12Al–40Fe, at different test temperatures. At 300 K, the alloy exhibited a yield strength of 507 MPa and a fracture stain of 28%. At 700 K, the yield strength decreased to ≈ 420 MPa and ε_f also decreased to 15%. At both 300 K and 700 K, necking preceded final failure and the work hardening rate was

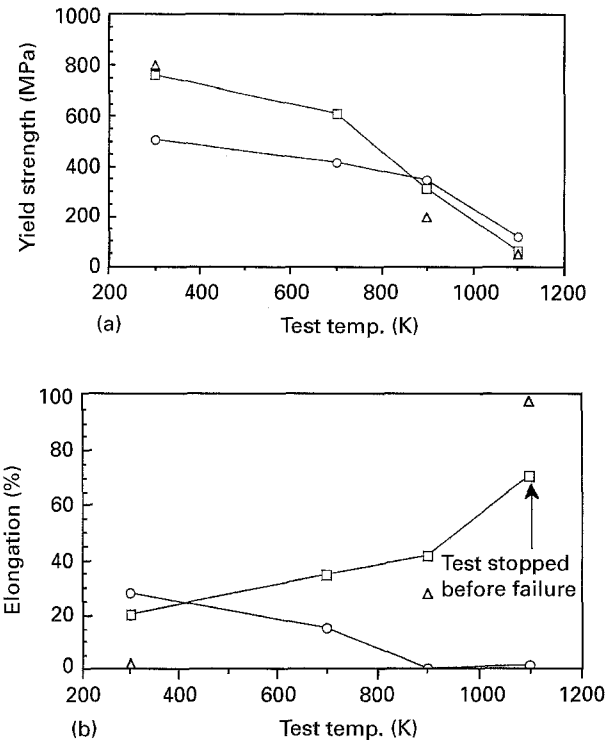

Figure 5 Graph of temperature dependence of (a) yield strength and (b) elongation of (□) multi-phase alloy NI–20Al–30Fe, (○) γ/γ′ phase Ni–12Al–40Fe and (△) β′ phase Ni–30Al–20Fe.

insensitive to the temperature change. At 900 K, the alloy failed in a brittle manner at a stress of ≈ 345 MPa immediately before 0.2% strain yield. At 1100 K, where the alloy is known to exhibit a coarsened γ/γ′ microstructure [10], a low yield strength of 119 MPa and $\approx 1\%$ fracture strain was observed. No work-hardening was observed at this temperature.

The stress–strain curves for the β′ alloy, Ni–30Al–20Fe, are shown in Fig. 4. At room temperature, a minimum fracture strain of $\approx 2\%$ was observed following yielding at a stress of 800 MPa (a second specimen exhibited $\approx 6\%$ elongation with a yield and ultimate stress of 825 and 1070 MPa, respectively [6]). At 900 K, the yield strength decreased to 199 MPa and ε_f increased to $\approx 27\%$. At 1100 K, the yield stength decreased further to only ≈ 53 MPa, but ε_f increased dramatically to 97%. No strain-hardening was observed in either elevated temperature test. The high ε_f at 1100 K is indicative of the contribution of the β′ phase towards the high ductility of the multi-phase alloy.

Fig. 5a summarizes the variation of the yield strength of the alloys with temperature, the datum point for the γ/γ′ alloy Ni–12Al–40Fe at 900 K represents the fracture stress at just below 0.2% plastic strain. The variation of yield strength with temperature was similar to the trends observed in hot hardness measurements for all the alloys. Fig. 5b summarizes the tensile elongation for the alloys as a function of temperature. While the elongation of the multi-phase alloy increased continuously with increasing temperature, the elongation of the γ/γ′ alloy shows a minimum at 900 K where the alloy failed around

yield. By contrast, the elongation of the β′ alloy increased continuously with increasing test temperatures. The high ductility of the multi-phase alloy at 900 K and 1100 K thus appears to arise from the increased ductility of the β′ phase, as shown in Fig. 5b.

3.3. Fractography

The fracture surfaces of the tensile-tested specimens were examined using a scanning electron microscope (Figs 6–8). For the multi-phase alloy, fracture at 700 K was similar to that previously observed at 300 K [8] consisting of transgranular cleavage failure in the pro-eutectic β′ phase and dimple fracture in the eutectic (Fig. 6a). At higher temperatures (Fig. 6b, c), the proeutectic β′ phase underwent a change from transgranular fracture to dimple fracture, indicating increased ductility for the β′ phase in the temperature range 700–900 K. This change coincides with the loss of hardness of the β′ alloy above ≈ 750 K and the increase in ε_f of the β′ phase to 27% at 900 K. The fracture surface at 1100 K was essentially similar to 900 K, although some large voids were observed on the fracture surface at 1100 K. Dimple fracture was observed in the eutectic at all test temperatures.

The fracture mode of the γ/γ′ alloy also changed with increasing temperature. Dimple fracture was previously observed at room temperature [8], Fig. 7a. This was replaced by a mixture of intergranular fracture and dimple fracture at 700 K, Fig. 7b, whereas at both 900 K and 1100 K, completely intergranular fracture occurred, Fig. 7c. The decreased ductility and intergranular fracture of Ni_3Al and $(Ni, Fe)_3(Fe, Al)$ alloys has been noted previously in the temperature range 873–1073 K and ascribed to the dynamic embrittlement of grain boundaries by ambient oxygen [15, 16].

The fracture surfaces of tensile-tested specimens of the β′ alloy also changed with temperature. Transgranular cleavage was noted at 300 K [8], while the fracture mode was intergranular fracture at 900 K and dimple fracture at 1100 K (Fig. 8). Note that, although the fracture was intergranular at 900 K, the individual grains showed evidence of plasticity (note the dimpled surface of individual grains in Fig. 8b). At 1100 K, extensive voiding was evident on the fracture surface. The results are similar to the observe fracture behaviour of pro-eutectic β′ phase in the multi-phase alloy.

Examination of back-scattered electron images of the polished longitudinal sections of the multi-phase alloy specimens tested at 700, 900 and 1100 K revealed cavities, the size of the cavities increasing with increasing test temperatures, see Fig. 9. Note that the γ/γ′ phase, which is richer in the higher atomic number elements, is the brighter phase. Fig. 9a shows that at 700 K, most voiding is limited to the grain boundaries and interphase interfaces. By contrast, the voids were almost exclusively in the γ/γ′ phase at 900 K, see Fig. 9b, and in the β′ phase at 1100 K, see Fig. 9c. The elongated structure of the pro-eutectic phase was observed to be replaced at 1100 K (Fig. 9d) by a more homogeneous and equiaxed microstructure. This observation with the large elongation observed for the multi-phase alloy at 1100 K, is indicative of a dynamically recrystallized microstructure.

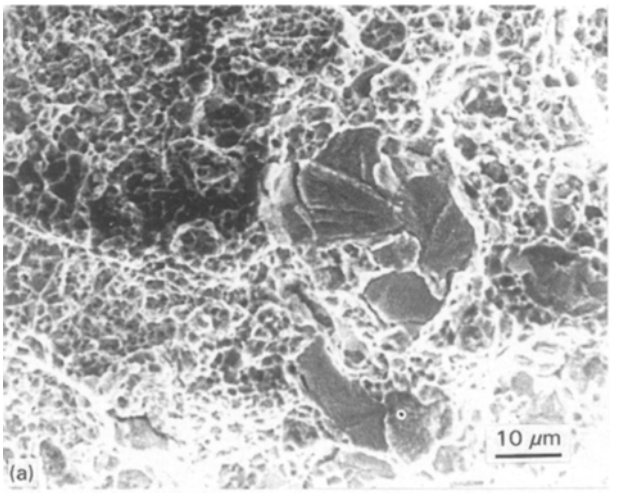

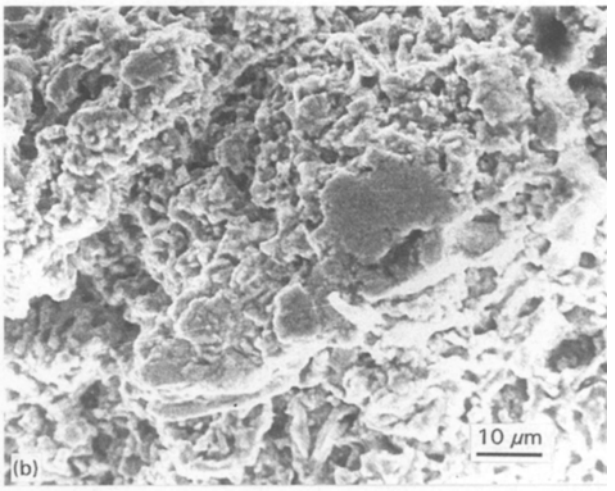

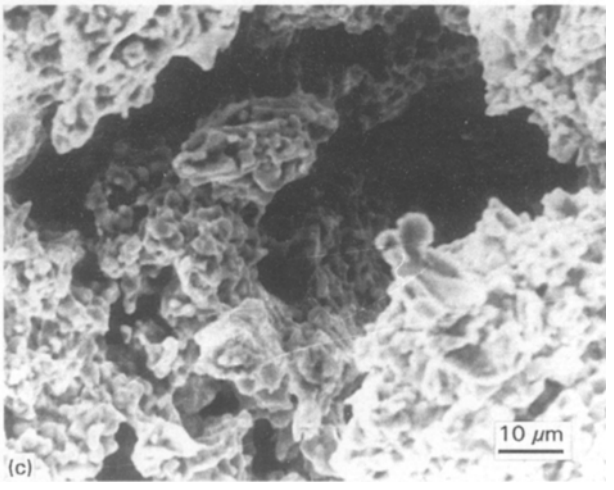

Figure 6 Fractographs of multi-phase alloy Ni–20Al–30Fe tested in tension at (a) 700 K, (b) 900 K and (c) 1100 K. The eutectic exhibits dimple fracture at all temperatures. The pro-eutectic β′ phase, by contrast, undergoes a change in fracture mode from transgranular cleavage at 700 K to dimple fracture at 900 K.

Polished longitudinal sections of the γ/γ′ alloy, Ni–12Al–40Fe, indicated the presence of grain boundary cracks at both 900 K and 1100 K, which is consistent with the intergranular fracture mode

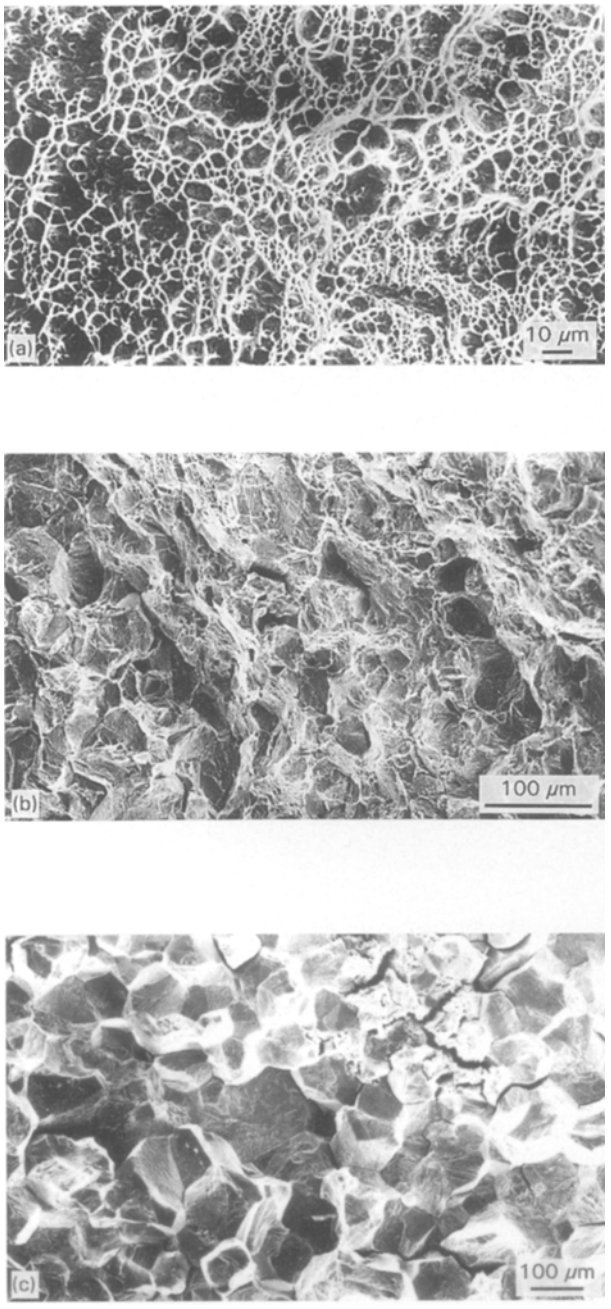

Figure 7 Fractographs of γ/γ′ alloy, Ni–12Al–40Fe, tested in tension at (a) 300 K [1], (b) 700 K and (c) 900 K. Fracture surface is dimpled at 300 K, mixed mode (dimple + intergranular) at 700 K, and completely intergranular at 900 and 1100 K.

observed for this alloy at these temperatures, see Fig. 10. Similarly, polished longitudinal sections of the β′ alloy, Ni–30Al–20Fe, tested at 900 K (Fig. 11a) indicated the presence of grain-boundary cracks, which is consistent with the observed fracture mode at this temperature; a few longitudinal cracks along the stress axis were also observed. These longitudinal cracks were also observed at room temperature [8] and are believed to be the result of prior processing (casting + extrusion). At 1100 K (Fig. 11b), however, extensive voiding was observed and the grain boundaries were no longer straight. The large voids observed in the micrograph are mostly situated at the grain boundaries and probably resulted from the coalescence of smaller voids nucleated by creep cavitation.

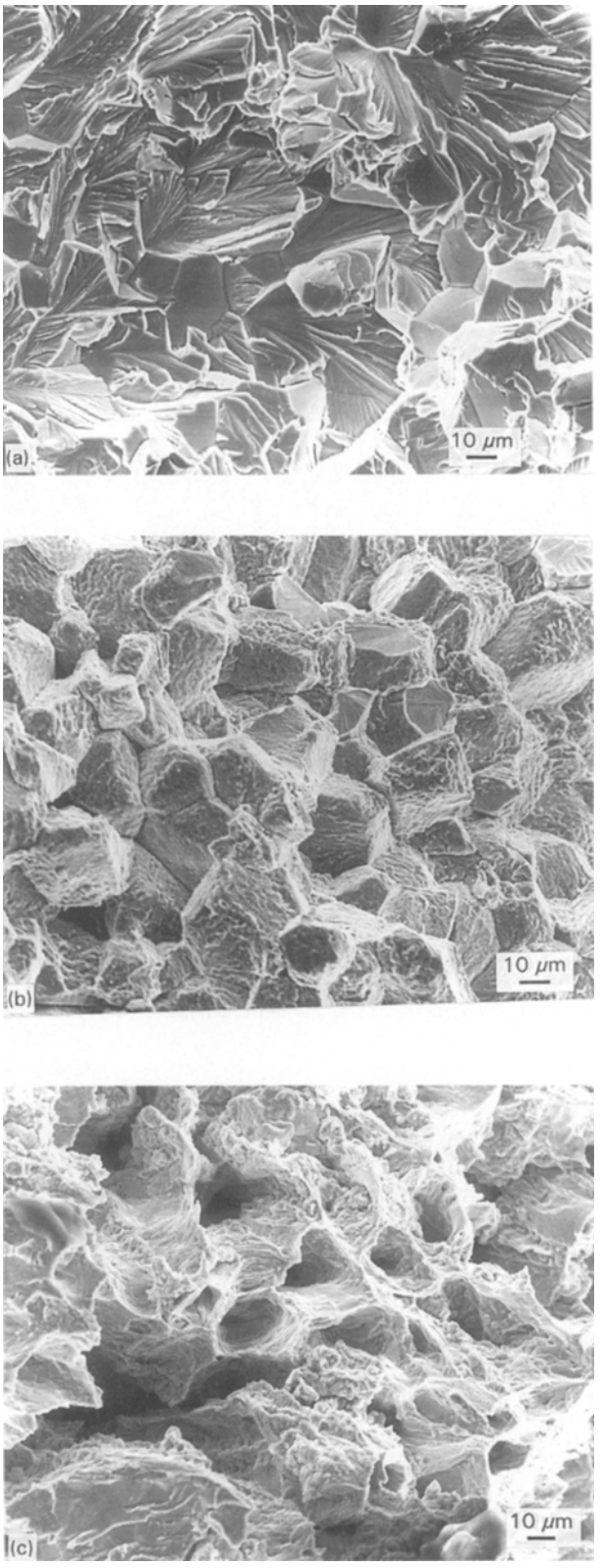

Figure 8 Fractographs of β′ alloy, Ni–30Al–20Fe, tested in tension at (a) 300 K [1] (b) 900 K and (c) 1100 K. The fracture is transgranular cleavage at 300 K, intergranular at 900 K and dimple fracture at 1100 K.

The curved grain boundaries (arrowed in Fig. 11b) indicate grain-boundary migration has occurred.

3.4. Deformation mechanisms

The room-temperature deformation behaviour of the cast and extruded multi-phase alloy and alloys similar

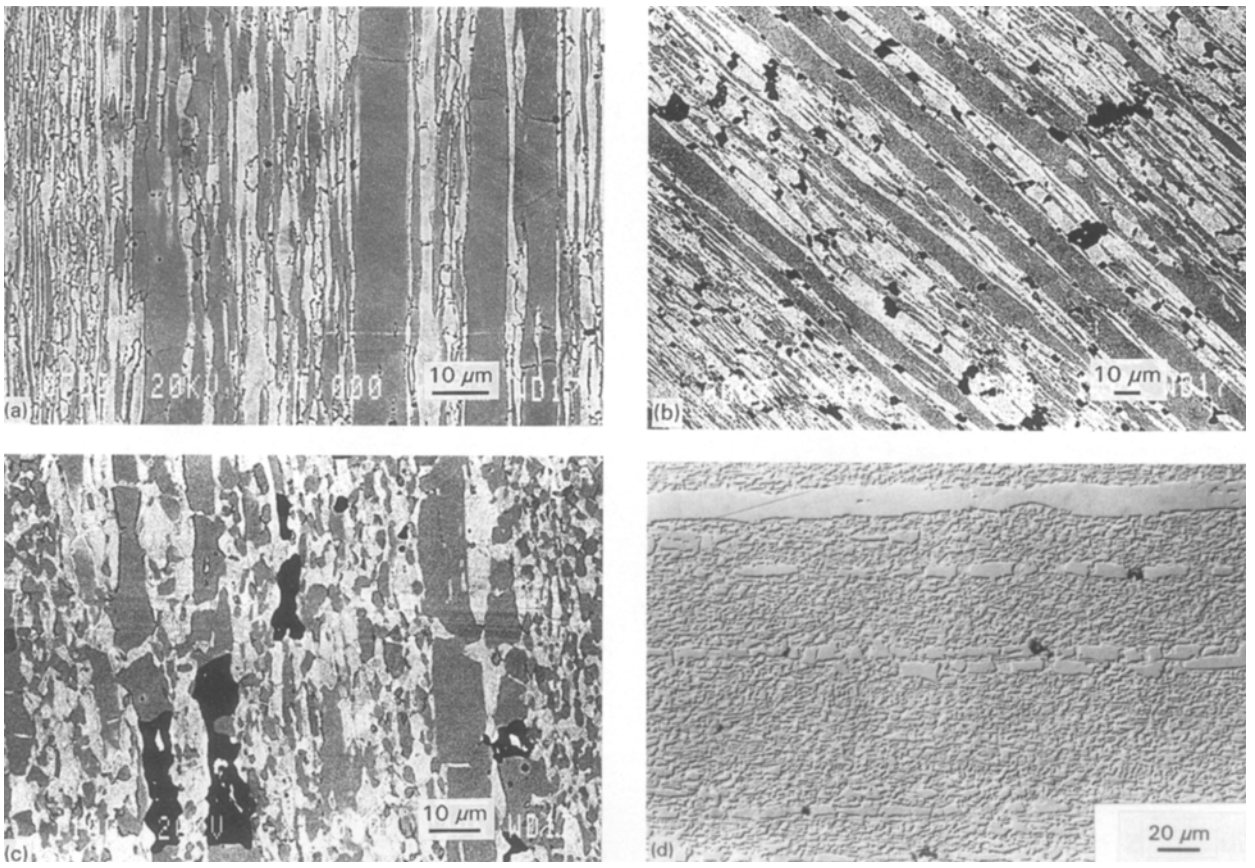

Figure 9 Backscattered electron images of polished longitudinal sections of Ni–20Al–30Fe tensile specimens tested in tension at (a) 700 K, (b) 900 K and (c) 1100 K. Voids were observed at 700, 900 and 1100 K, their size increasing with increasing temperatures. At 700 K, the fine voids were limited to the grain boundaries and interphase interfaces. AT 900 K, the voids were concentrated in the brighter (γ/γ') phase, while at 1100 K, the voids were observed in the darker (β') phase. (d) Optical micrograph of polished longitudinal section of tensile specimen tested at 1100 K showing the coarse pro-eutectic phase breaking down into finer units.

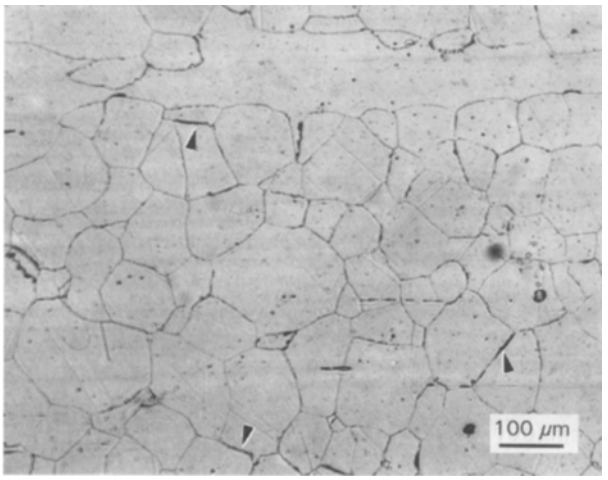

Figure 10 Optical micrograph of polished longitudinal section of γ/γ' alloy Ni–12Al–40Fe, tested in tension at 900 K. Grain-boundary cracks are observed (arrowed).

to its constituents phases have been reported elsewhere [6, 8]. Briefly, the observed operative slip vector in the β' alloy and the pro-eutectic β' phase of the multi-phase alloy was $\langle 1\,0\,0\rangle$. The Burgers' vector of dislocations in the γ/γ' alloy and in the γ/γ' phase of multi-phase alloy was observed to be $\langle 1\,1\,0\rangle$ [8], the $1/2\langle 1\,1\,0\rangle$ dislocation partials were easily resolvable.

Thin foils from gauge sections of the multi-phase alloy samples strained to failure at 700 and 900 K, and strained up to 70% at 1100 K were examined in the TEM. For samples tested at 700 K, a high dislocation density was observed in both the β' and γ/γ' phases. The dislocation densities in both β' and γ/γ' phases were, however, observed to decrease with increasing test temperatures (see, for example, Fig. 12a–c for the β' alloy Ni–30Al–20Fe). At 1100 K, despite rapid cooling from the test temperatures, the deformed microstructure had a very low dislocation density. Low-angle boundary formation was observed within the deformed grains of both β' and γ/γ' phases at 900 and 1100 K, indicating that dynamic recovery processes contribute to the elevated temperature deformation of the multi-phase alloy. Dynamic recrystallization in the β' phase at 1100 K could have occurred but could not be proved unambiguously due to the difficulty in differentiating new, dynamically-recrystallized, dislocation-free grains from prior existing small (≈ 0.5 μm width) β' grains with a dynamically-recovered deformation substructure. However, as noted earlier, optical micrographic observations (Fig. 9d) do indicate the occurrence of dynamic recrystallization in the pro-eutectic β' phase at 1100 K. Furthermore, grain-boundary migration (which is usually indicative of dynamic recrystallization processes) observed in the β' alloy, Ni–30Al–20Fe, deformed at 1100 K to failure

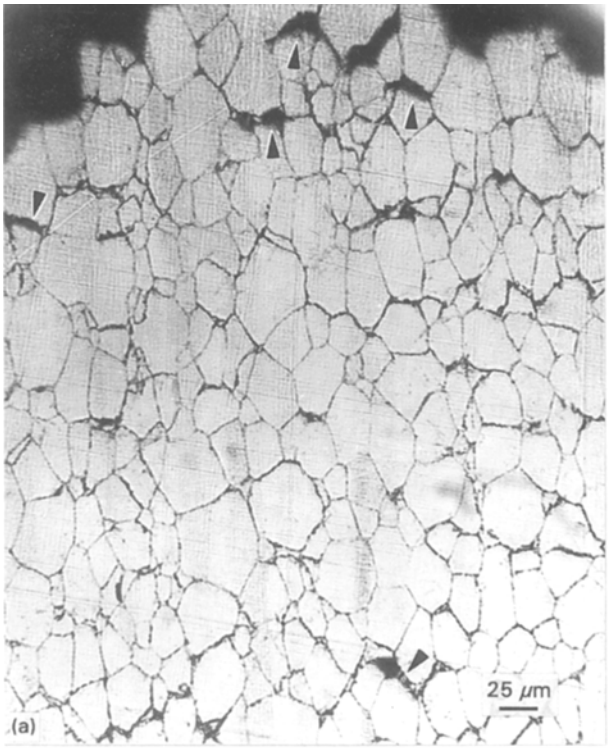

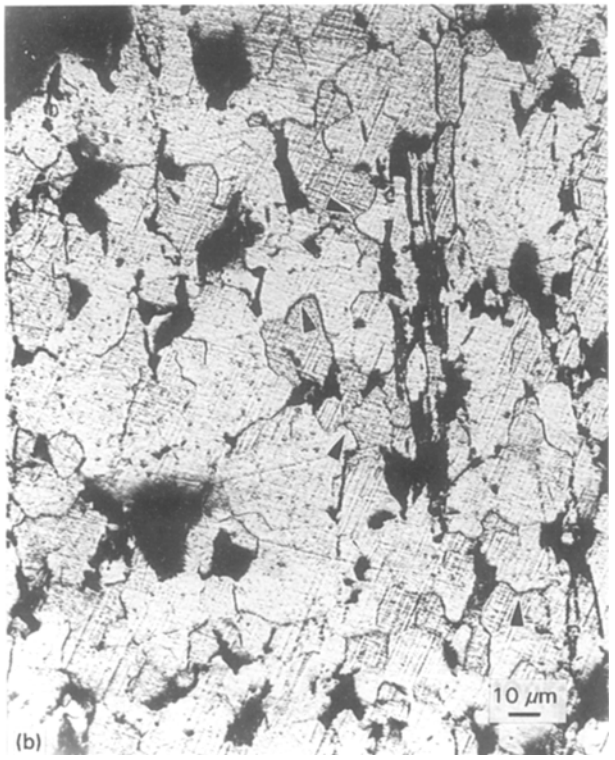

Figure 11 Optical micrographs of polished longitudinal sections of β′ alloy Ni–30Al–20Fe, tensile-tested in tension at (a) 900 K and (b) 1100 K. Grain-boundary cracks are observed at 900 K (arrowed), while at 1100 K extensive voiding and grain boundary migration (arrowed) were observed.

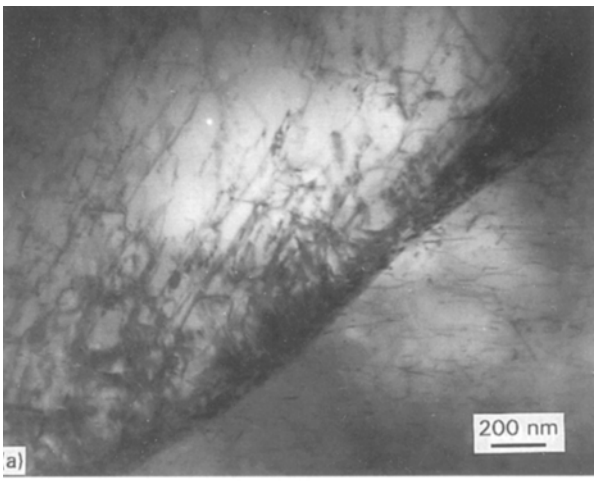

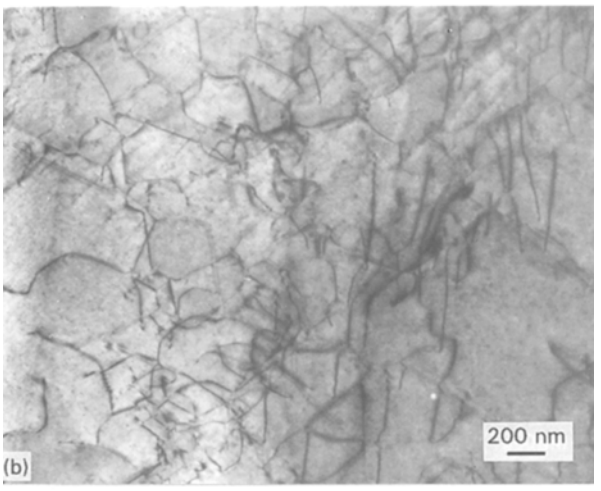

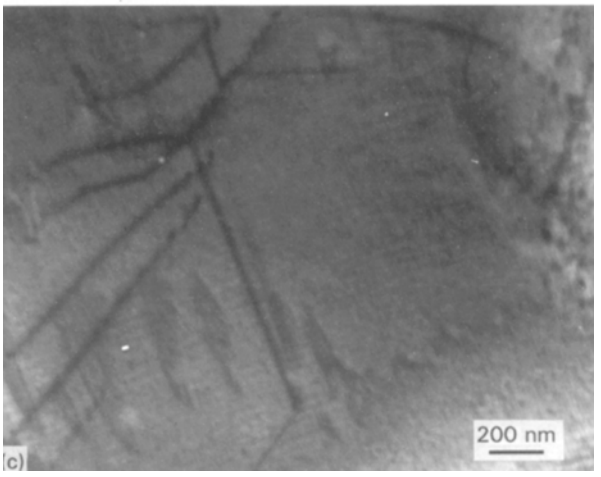

Figure 12 Bright-field transmission electron micrographs of β′ alloy Ni–30Al–20Fe deformed (a) 2% at room temperature, (b) ~ 27% at 900 K, (c) ~ 97% at 1100 K. Note the decrease in dislocation density with increasing deformation temperature.

(Fig. 11b) would also support such a conclusion. Thus, while dynamic recovery processes are active in both β′ and γ/γ′ phases during the deformation of the multiphase at 900 K and 1100 K, it is possible that dynamic recrystallization also occurs in the β′ phase.

For the β′ alloy, thin foils from tensile specimens strained to failure (≈ 27% strain) at 900 K (Fig. 12b) exhibited a lower dislocation density that observed for ≈ 2% strain at room temperature (Fig. 12a); sub-grain formation was also observed. Thin foils from gauge sections of samples strained 97% at 1100 K (Fig. 12c) exhibited an even lower dislocation density; again, sub-grains were observed. These observations are indicative of dynamic recovery processes being

operative in the β′ alloy at both 900 and 1100 K. These observations are consistent with the observations for the β′ component of the multi-phase alloy reported above.

In order to determine the slip vectors of dislocations in the samples strained at 1100 K, a multi-phase alloy specimen was strained 5%, and thin foils were prepared from its gauge and analysed in the TEM. The microstructure consisted mostly of grains with very low dislocation density. Fig. 13 shows a dislocation network in the β′ phase along with two individual dislocations imaged with different diffraction vectors. The individual dislocations marked a and b and the segments of the dislocation network marked c, g and I, are in contrast when imaged with $\boldsymbol{g} = 1\,0\,1$ and $0\,1\,1$ and out of contrast with $\boldsymbol{g} = 0\,2\,0$, $2\,0\,0$ and $1\,1\,0$, indicating a [0 0 1] Burgers' vector. By contrast, the segment marked e was in contrast with $\boldsymbol{g} = 0\,2\,0$, $1\,0\,1$ and $1\,1\,0$ and out of contrast with $\boldsymbol{g} = 0\,1\,1$ and $2\,0\,0$, indicating a [0 1 1] Burgers' vector, see Fig. 13a–c. Similarly, the dislocation segments h, i and j exhibit contrast consistent with [1 0 0], [0 0 1] and [1 0 1] Burgers' vector which satisfies the dislocation reaction i + h → j. The observed residual contrast of the dislocations when the invisibility criteria for screw $\boldsymbol{g}\cdot\boldsymbol{b} = 0$ or edge dislocations $\boldsymbol{g}\cdot\boldsymbol{b} = 0$ and $\boldsymbol{g}\cdot\boldsymbol{b}\times\boldsymbol{u} = 0$ were satisfied was probably due to the high elastic anisotropy of the β′ alloy.

Fig. 14 shows a dislocation network in the γ/γ′ phase of the multi-phase alloy deformed at 1100 K. The dislocations were found to be of ⟨1 1 0⟩ type which, again, is similar to the room-temperature observations [8]. It should be noted, however, that at 1100 K the dislocations are single 1/2⟨1 1 0⟩ dislocations, which is consistent with the microstructure of the phase being γ only rather than γ/γ′ (see [10]).

Because the Burgers' vector of dislocations strained at 300 K and 1100 K are similar in both the β′ and γ/γ′ phases, it would be reasonable to presume similar deformation mechanisms being operative at the intermediate temperatures 700 K and 900 K.

4. Discussion

The hot-hardness and tensile test data indicate that while the strength of the β′ alloy decreases with increasing temperature, the γ/γ′ alloy retains its strength up to 973 K: unlike some γ′-based alloys, no anomalous strengthening was observed for the γ/γ′ alloy. The multi-phase alloy exhibits a behaviour intermediate between that of its constituent phases. Thus, while at room temperature its yield strength (≈ 760 MPa) is similar to that of the β′ alloy (≈ 800 MPa) rather than that of the γ/γ′ alloy (yield strength (≈ 500 MPa), at 900 K where the β′ alloy exhibits less strength (≈ 200 MPa), its strength (≈ 310 MPa) is similar to that of the γ/γ′ alloy (≈ 345 MPa). Similarly, while the room-temperature elongation of 20% is similar to that of the γ/γ′ alloy (which exhibits ≈ 28% elongation), at higher temperatures, where the γ/γ′ alloy is brittle ($\varepsilon_f < 1\%$), the ductility of the multi-phase alloy (34% and 100% at 900 and 1100 K, respectively) is similar to that of the β′ alloy (27% and 97%). This indicates that over the temperature range 300–1100 K, the multi-phase alloy mitigates the problems associated with each of its constituents phases at any particular temperature. The poor strength of the multi-phase alloy at $T > 1100$ K can be ascribed to both the poor elevated temperature strength of the β′ constituent phase as well as the dissolution/disordering of γ′ particles and lack of anomalous strengthening of the γ′ phase.

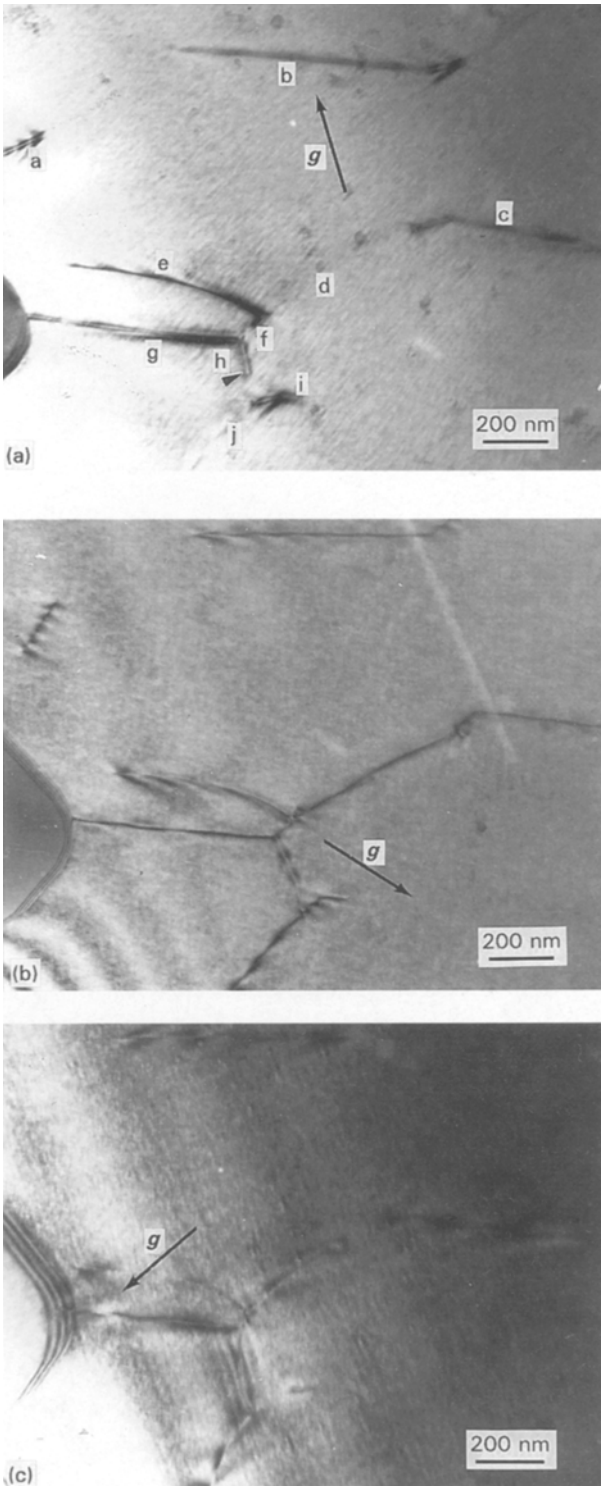

Figure 13 Dislocations in the β′ phase in extruded multi-phase Ni–20Al–30Fe, strained ~ 5% at 1100 K and air-cooled to room temperature. Imaging conditions: (a) $\boldsymbol{g} = (0\,2\,0)$, (b) $\boldsymbol{g} = (0\,\bar{1}\,1)$, and (c) $\boldsymbol{g} = (2\,0\,0)$. Beam direction near [1 0 1] for (a), near [1 1 1] for (b) and near [0 0 1] for (c).

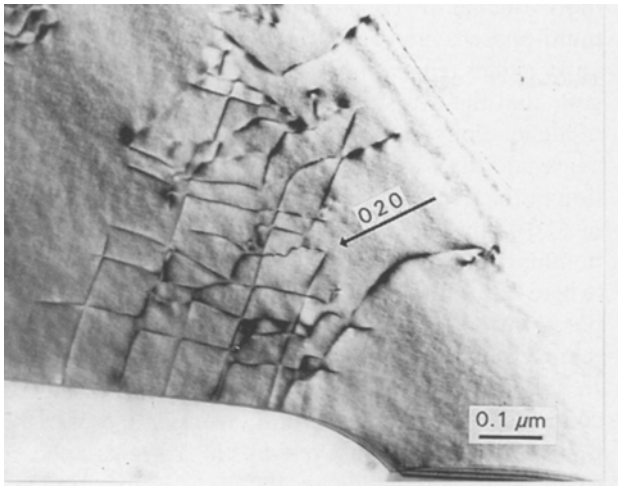

Figure 14 Dislocations in the γ phase in extruded multi-phase Ni–20Al–30Fe, strained ~ 5% at 1100 K and air-cooled to room temperature. Imaging conditions: $\boldsymbol{g} = (0\,2\,0)$. Beam directions near [0 0 1].

The yield strength of directionally solidified (DS) Ni–20Al–30Fe was measured in compression over the temperature range 100–900 K [17]. The room-temperature microstructure consisted of coarse lamellae (≈ 5 μm lamellae width) of β′ and γ/γ′ phases. 'The phases observed at room temperature were similar to those observed by Guha *et al.* [8], who processed their alloys through a casting and extrusion route, and those of Huang *et al.* [18], who studied rapidly solidified ribbons. While the elevated temperature behaviour for the DS alloy was similar to that reported in this study, the room-temperature yield strength (≈ 500 MPa) and tensile elongation (≈ 10%) were lower than the yield strength (≈ 760 MPa) and tensile elongation (≈ 20%) reported by Guha *et al.* [8]. The differences in room-temperature tensile ductility are probably related to differences in the scale and distribution of constituent phases in the microstructure; the smaller (0.5 μm) lamellae width and more homogeneous distribution of the ductile and less ductile phases within the cast and extruded alloy contribute to a greater degree of crack arrest [8] and to improved deformation transfer mechanisms [9] operating within the β′-γ/γ′ aggregate, thereby delaying fracture within the less ductile β′ phase. This, in turn, contributes to the greater ductility of the multi-phase aggregate.

The variation of the yield strength with temperature for the cast + extruded β′ alloy is similar to that of both stoichiometric and off-stoichiometric NiAl alloys [11, 12], and also that of Ni–30Al–20Fe–0.05Zr processed by a powder metallurgy (P/M) route [19]. In contrast to the cast + extruded alloy which exhibited a minimum of 2% elongation (and up to 6% elongation [6]) at room temperature, the P/M alloy exhibited fracture before yield between 300 and 600 K and a brittle-to-ductile transition temperature of ≈ 1000 K. On the other hand, the P/M-processed alloy also exhibited superior strength retention at elevated temperatures, e.g. $\sigma_y \approx 350$ MPa at 900 K compared to 200 MPa for the cast + extruded alloy. The higher strength retention and lower ductility of the P/M-processed alloy may be attributed to the processing route which probably produced oxide contaminants at grain boundaries.

While the mechanical behaviour of the β′ alloy examined here is typical of B2 alloys, the mechanical behaviour of the γ/γ′ alloy is worth further comment. Horton *et al.* [16] studied the elevated temperature mechanical behaviour of some Ni–Fe–Al γ′-based alloys containing up to 20 at % iron and reported a positive temperature dependence of yield strength in each case. The degree of anomalous strengthening (i.e. difference in strength between 873 K and room temperature) was approximately concentration-independent for up to 10 at % iron, but decreased for alloys with higher iron concentrations. For example, the alloy Ni–15Al–20Fe exhibited nearly the same yield strength at 300 and 873 K. If this trend is assumed to continue for higher iron concentrations, the lack of any positive temperature dependence of yield strength for the γ/γ′ alloy Ni–12Al–40Fe is not surprising. Beardmore *et al.* [20] have shown that for Ni–Cr–Al γ/γ′ alloys the degree of anomalous strengthening is sensitive to the volume fraction of γ′ precipitates, increasing with an increasing volume fraction of precipitates. The observed behaviour of Ni–12Al–40Fe is similar to low (about 10%–20%) γ′ volume fraction Ni–Al–Cr alloys [20]. However, the volume fraction of γ′ precipitates in Ni–12Al–40Fe is much higher (see [10]). Thus the observed lack of anomalous strengthening probably reflects the intrinsic behaviour of the alloy, i.e. the difference between Ni–Al–Cr versus Ni–Al–Fe γ′ precipitates. Horton *et al.* [16] have also noted an increase in yield strength with increasing iron concentration. However, the room-temperature strength of Ni–15Al–20Fe (637 MPa) examined by these workers was higher than that of Ni–12Al–40Fe (507 MPa) examined here, indicating the deleterious effect of very high iron concentrations (or low aluminium concentrations) on the mechanical properties of γ′ phases. The ductility drop at elevated temperature for the γ/γ′ alloy Ni–12Al–40Fe was also present in the alloys studied by Horton *et al.* [16]. While the effect has often been ascribed to dynamic embrittlement by oxygen [15, 16], the observation of voids at 900 K which was limited to only the γ/γ′ phase in the multi-phase alloy, which would be shielded from ambient oxygen by the β′ phase, indicates the possibility that the brittle behaviour is intrinsic to this alloy at intermediate temperatures. By contrast, despite the $\varepsilon_f \approx 1\%$ at 1100 K for the γ/γ′ alloy, no voids are observed within the γ/γ′ phase of the multi-phase alloy strained to $\varepsilon_f > 70\%$, indicating that the embrittlement at 1100 K is possibly related to dynamic embrittlement by oxygen. For alloys containing up to 20 at % iron, Horton *et al.* [16] observed that the embrittlement was most severe at 1123 K, which is consistent with the observations reported here.

Turning now to the deformation modes, Guha *et al.* [8] and Huang *et al.* [18] have examined the room-temperature deformation mechanisms in the β′ and γ/γ′ phases of cast + extruded and rapidly solidified Ni–20Al–30Fe respectively. Guha *et al.* [8] reported

that the β′ and γ/γ′ phases deform by movement of ⟨1 0 0⟩ dislocations and ⟨1 1 0⟩ dislocations, respectively. By contrast, Huang *et al.* [18] reported the observation of a few ⟨1 1 1⟩ dislocations among a majority of ⟨1 0 0⟩ dislocations in the β′ phase of rapidly solidified Ni–20Al–30Fe. The data presented here indicate that the primary deformation mechanism for the β′ phase, namely glide of ⟨1 0 0⟩ dislocations, does not change between 300 and 1100 K, although ⟨1 1 0⟩ dislocations arising from the interaction of ⟨1 0 0⟩ dislocations may contribute to the deformation of β′ phase at higher temperatures. Similar observations of ⟨1 1 0⟩ dislocations in NiAl deformed at elevated temperatures have been noted by Lloyd and Loretto [21], Zaluzec and Fraser [22], Lasalmonie [23] and Baker and Schulson [24]. Mobile segments of ⟨1 1 0⟩ dislocations may alleviate the strain incompatibilities at the grain boundaries resulting from only three independent slip systems provided by the operative ⟨0 0 1⟩ slip [25] (as opposed to five required by von Mises criterion [26] for general plastic deformation) by providing additional slip systems. By contrast, Ball and Smallman [27] have suggested that elevated temperature deformation occurs through climb and cross-slip of ⟨1 0 0⟩ dislocations. Such a suggestion would also be difficult to rule out in view of the dependence of T_t on melting point noted earlier. It is possible that both the above mechanisms are active in the elevated temperature deformation of the β′ alloy. For the γ/γ′ phase, deformation occurs by the motion of paired 1/2⟨1 1 0⟩ dislocations at low temperature, but individual 1/2⟨1 1 0⟩ dislocations at elevated temperatures, when disordering has occurred.

Because the volume fraction of the β′ phase (both pro-eutectic and eutectic β′ constituent) between 300 and 1100 K comprises approximately two-thirds of the multi-phase aggregate, it would appear that the strength of the multi-phase alloy cannot be described well by a simple rule-of-mixture approach. This is evident in Fig. 5a where the yield strength of the multi-phase aggregate at each temperature is always closer to the strength of the stronger phase rather than a weighted average of the strength of the constituent phases. This can probably be ascribed to the differences in the scale of the microstructure between the β′ and γ/γ′ grains within the multi-phase alloy and those of the β′ and γ/γ′ alloy themselves; the β′ and γ/γ′ grains within the multi-phase alloy are approximately an order of magnitude smaller in size compared to the alloys Ni–30Al–20Fe (β′) and Ni–12Al–40Fe (γ/γ′). Clearly, some strengthening is expected due to the smaller grain sizes (Hall–Petch type strengthening) which may partially offset the strength loss due to the γ/γ′ grains at lower temperatures and the β′ grains at higher temperatures.

More interestingly at room temperature, despite the volume fraction of the γ/γ′ phase being only ~ 33%, the ductility of the multi-phase aggregate is similar to that of the γ/γ′ alloy itself. At higher temperatures (900 K), where the β′ and γ/γ′ constituents interchange their roles as the strengthener and the ductilizer, respectively, the elongation of the multi-phase matrix is still greater than the elongation of the more ductile β′ constituent, see Fig. 5b. That the multi-phase aggregate is indeed capable of significantly higher elongation at each test temperature suggests that the β′ and γ/γ′ phases are, perhaps, capable of higher elongation-to-failure within the multi-phase aggregate than by themselves. Because the deformation in the β′ phase is accomplished by the movement of ⟨1 0 0⟩ dislocations at all temperatures, any grain-boundary strain incompatibility at low temperatures (where diffusion-assisted processes are not active) imposed by the limited number of slip systems is perhaps removed by the presence of neighbouring γ/γ′ grains. *In situ* TEM straining experiments [9] have indeed confirmed such deformation transfer across the β′–γ/γ′ interfaces, where pile-ups in β′ grains appears to nucleate slip bands in the γ/γ′ grains. Equally interesting, perhaps, is the high ductility of the multi-phase aggregate at 900 K where the γ/γ′ component is brittle. Because the γ/γ′ phase deforms by ⟨1 1 0⟩ slip, which does not suffer from any limitation on the number of operative slip systems, the presence of the more ductile β′ phase, thus cannot help improve the ductility of the γ/γ′ phase (the brittleness is rather more intrinsic). It is suggested that the ductility of the multi-phase aggregate arises primarily from the ductility of the β′ phase with the fractured γ/γ′ pieces being held together and carried within the more ductile matrix. This is evident from the scanning electron micrograph in Fig. 9b where large voids are seen in the γ/γ′ (brighter) phase.

In contrast to the behaviour at 900 K, the superplastic behaviour of the multi-phase alloy at 1100 K, despite the limited strain-to-failure of the constituent γ/γ′ phase, cannot solely be ascribed to the ductility of the β′ phase. The limited strain-to-failure of the γ/γ′ alloy at 1100 K where the microstructure is disordered [10] and the operative deformation system is 1/2⟨1 1 0⟩ dislocations, is surprising. Thus, the embrittlement at 1100 K is quite possibly related to dynamic embrittlement by oxygen [15, 16] which would be consistent with observations by Horton *et al.* [16] in similar Ni–Fe–Al intermetallics at 1100 K. Given that the γ/γ′ constituent is not intrinsically brittle at 1100 K, the extensive ductility of the multi-phase alloy could thus be related to the ductility of both β′ and γ/γ′ constituents; the ductility of the γ/γ′ constituent itself could possibly be related to the shielding effect of the more protective β′ constituent. That no voids are observed within the γ/γ′ constituent in the multi-phase alloy deformed at 1100 K, see Fig. 9c, is consistent with such a suggestion. Thus, in addition to alleviating brittleness by removing incompatibilities resulting from a limited number of slip systems, the multi-phase alloy approach is also capable of improving the ductility by alleviating environmental effects.

5. Conclusions

Mechanical testing, fractography, optical and scanning electron microscopy of polished longitudinal sections and transmission electron microscopy of thin foils from deformed samples of the multi-phase alloy

and alloys similar to it constituent phases have shown that:

1. the β′ alloy Ni–30Al–20Fe exhibits behaviour typical of a B2 compound [13], namely a yield strength plateau (at ≈ 800 MPa) up to ≈ 700 K after which the yield strength decreased rapidly, and steadily increasing ductility (from ≈ 2% at room temperature) with increasing temperature;

2. the γ/γ′ alloy Ni–12Al–40Fe exhibited a gradual decrease in strength (from 507 MPa at room temperature) with increasing temperatures up to 900 K, above which the strength decreased rapidly due to coarsening of the γ/γ′ microstructure (see [10]) and eventual dissolution of γ′ precipitates. The failure strain was high at low temperature (28% elongation at room temperature), but a ductility drop occurred at elevated temperature (to < 1% elongation), a feature observed in several related alloys [16];

3. the yield strength of the multi-phase alloy Ni–20Al–30Fe decreased slowly from 760 MPa at room temperature to 310 MPa at 900 K, after which it decreased rapidly. This behaviour was similar to that of its constituent phases. In contrast, the alloy exhibited good ductility at all temperatures, indicating that the arrangement of the constituent phases could ameliorate the inherent brittleness of individual phases.

4. slip was by ⟨1 0 0⟩ dislocation in the β′ phase at all temperatures, although ⟨1 1 0⟩ dislocations were also observed at 1100 K. Slip in the γ/γ′ phase was by paired 1/2⟨1 1 0⟩ dislocations at low temperature but by single 1/2⟨1 1 0⟩ dislocations at elevated temperatures where the γ′ had dissolved.

Acknowledgements

The authors gratefully acknowledge the assistance of Dr M.V. Nathal, Dr J.D. Whittenberger, Dr I. Locci, Dr S.V. Raj, Dr R.D. Noebe, Dr F. Lemkey, Mr D.J. Gaydosh and Mr D. Deadmore in materials processing and hot-hardness testing. The assistance of Mr R. Davies, Met-Lab, NASA-Lewis, and Dr C. Daghlian, Dartmouth Rippel Electron Microscope Center, is also acknowledged. This research was supported by NAG-3-775, contract monitor Dr M.V. Nathal.

References

1. E. P. GEORGE and C. T. LIU, *J. Mater. Res.* **5** (1990) 754.
2. P. NAGPAL and I. BAKER, *Mater. Charact* **27** (1991) 167.
3. K.H. HAHN and K. VEDULA, *Scripta Metall.* **23** (1989) 7.
4. P. NAGPAL and I. BAKER, *ibid.* **24** (1990) 2381.
5. S. GUHA, P. R. MUNROE and I. BAKER, *ibid.* **23** (1989) 897.
6. S. GUHA, I. BAKER, P. R. MUNROE and J. R. MICHAEL, *Mater. Sci. Eng.* **A152** (1992) 2588.
7. S. GUHA, P. R. MUNROE and I. BAKER, *Proc. MRS* **133** (1989) 533.
8. *Idem, Mater. Sci. Eng.* **A131** (1991) 27.
9. I. BAKER, S. GUHA and J. A. HORTON, *Philos. Mag.* **A67** (1993) 663.
10 S. GUHA, I. BAKER and P. MUNROE, *Mater. Charact* (1995) in press.
11. A. Z. ROZNER and WASILEWSKI, *J. Inst. Metals* **94** (1996) 169.
12. R. T. PASCOE and C. W. A. NEWEY, *Met. Sci.* **2** (1968) 138.
13. I. BAKER and P. R. MUNROE, in "High Temperature Aluminides and Intermetallics", edited by S. H. Whang, C. T. Liu, D. P. Pope, J. P. Steigler (TMS, Indianapolis, IN, 1990) p. 425.
14. M. F. SINGLETON, J. L. MURRAY and P. NASH, in "Binary Alloy Phase Diagrams I", edited by T. B. Massalski (ASM, Metals Park, OH, 1986) p. 142.
15. C. T. LIU, C. L. WHITE and E. H. LEE, *Scripta Metall.* **19** (1985) 1247.
16. J. A. HORTON, C. T. LIU and M. L. SANTELLA, *Metall. Trans.* **18A** (1987) 1265.
17. R. D. NOEBE, R. R. BOWMAN, J. T. KIM, M. LARSEN and R. GIBALLA, in "High Temperature Aluminides and Intermetallics" edited by S. H. Whang, C. T. Liu, D. P. Pope and J. P. Steigler (TMS, Indianapolis, IN, 1990) p. 271.
18. S. C. HUANG, R. D. FIELD and D. D. KRUEGER, *Metall. Trans.* **21A** (1990) 959.
19. S. V. RAJ, R. D. NOEBE and I. E. LOCCI, in "High Temperature Ordered Intermetallic Alloys IV", edited by Johnson, B. P. Pope and J. P. Steigler, Materials Research Society Symposium Proceedings, Vol 213 (MRS, 1991) p. 673.
20. P. BEARDMORE, R. G. DAVIES and T. L. JOHNSTON, *Trans. AIME* **245** (1969) 1537.
21. C. H. LLOYD and M. H. LORETTO, *Phys. Status Solidi* **39** (1970) 163.
22. N. J. ZALUZEC and H. L. FRASER, *Scripta Metall.* **8** (1974) 1049.
23. A. LASALMONIE, *J. Mater. Sci.* **17** (1982) 2419.
24. I. BAKER and E. M. SCHULSON, *Metall. Trans.* **15A** (1984) 1129.
25. G. W. GROVES and A. KELLY, *Philos. Mag.* **8** (1963) 877.
26. R. VON MISES, *Z. Agnew Math. Mech. S.* (1928) 161.
27. A. BALL and R. E. SMALLMAN, *Acta. Metall.* **14** (1966) 1517.

Received 1 May
and accepted 7 November 1995